AN OVERVEW OF THE KECK INTERFEROMETER NULLER

Eugen Serabyn[1]

[1] *Jet Propulsion Laboratory 171-113, California Institute of Technology, Pasadena CA 91109 (USA)*
gene.serabyn@jpl.nasa.gov

ABSTRACT

The first high dynamic range interferometry mode planned to come on line at the Keck Observatory is mid-infrared nulling interferometry. In this paper, an overview is given of the goals and experimental configuration of the Keck Interferometer Nuller (KIN). After an introduction to the science enabled by mid-infrared nulling interferometry on the Keck Interferometer's baseline, a system level overview of the experiment is provided, which includes a discussion of the optical path-length matching and stabilization approaches. This is followed by brief tours of both the nulling beam-combiner breadboard and the mid-infrared camera to be used in the experiment. The paper concludes with a discussion of the performance levels attained to date with the mid-infrared nullers built at the Jet Propulsion Laboratory. These symmetric nullers, all based on the modified Mach-Zehnder beam-combiner configuration, have now experimentally verified the predicted dual-polarization nulling capability of a reversed beamsplitter pair arrangement. To date, the JPL nulling beamcombiners have nulled broadband thermal mid-infrared radiation to the 10^{-4} level, and monochromatic (10.6 μm CO_2 laser) radiation to the 10^{-6} level.

1. INTRODUCTION

The advent of ten-meter class optical/infrared telescopes, as well as the increasing maturity of interferometric techniques at these wavelengths, is at last opening the door to high-dynamic range optical/infrared astronomical interferometry. The soon to be implemented experimental approaches include high-accuracy visibility measurements, measurements of wavelength-dependent phase shifts (differential phase), and infrared nulling interferometry.

The first interferometer to be able to exploit several of these high-dynamic range possibilities will be the Keck Interferometer, which combines the light from the twin Keck telescopes on Mauna Kea, HI (Fig. 1). Basic near-infrared visibility measurements are already being made regularly made with the Keck Interferometer, and several results are proceeding to publication. The next step will be to implement the high-dynamic-range observing modes, and of these, the next experimental mode slated for implementation on the summit of Mauna Kea is mid-infrared nulling. This paper presents an overview of the design of the Keck Interferometer Nuller (KIN), and provides an update on the instrumentation's current status.

Fig. 1. The Keck Observatory on Mauna Kea, HI, at latitude +19.826°. The baseline between the telescopes is 85 m in length, and is oriented 37.7° East of North.

2. NULLING INTERFEROMETRY GOALS

The basis of nulling interferometry is the interference of light from multiple telescopes so as to position a deep and achromatic destructive interference fringe across a target star, in order to reduce the brightness contrast ratio between the (residual) stellar flux and any sources in the star's immediate vicinity. This technique should thus open the door to the observation of potential exo-zodiacal disks and exo-planets around nearby stars, and indeed, early observations of binary stars and dust shells around evolved stars with short nulling baselines have begun to bear the approach out.

The basic design requirement set for the performance of the KIN is the ability to detect exozodiacal disks around nearby stars down to levels as faint as ten times the brightness of our solar system's own mid-infrared (10 μm) zodiacal emission. Such an exozodiacal disk would nevertheless still be on the order of a thousandth as bright as the parent star, and so the KIN instrumentation must then be capable of nulling stars to comparable part-in-a-thousand levels.

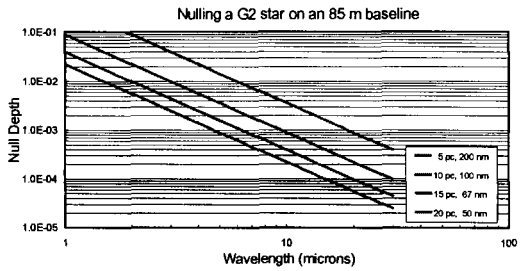

Fig. 2. Stellar-diameter-limited null depths for the Keck Interferometer for G2 stars at 5 – 20 pc distance. The inset shows the necessary path-length stability level.

Even for an ideal instrument, finite stellar diameters limit the attainable null depths, and the resultant null depth is then a function of stellar diameter and distance, as well as of the baseline length. Fig. 2 shows the infrared null depths attainable with the 85 m baseline available at the Keck Observatory for G2 stars in the 5 to 20 pc distance range. Also shown is the requisite level of pathlength stabilization. As can be seen in the figure, for stars at a canonical distance of 10 pc, null depths of about 10^{-3} are possible near wavelengths of 10 μm.

However, off-axis emission from exozodiacal disks or bright planets near constructive fringe peaks will be transmitted by the interferometer's fringe pattern, as in Fig. 3. For incidence normal to the baseline, the fringe spacing in the target 10-12 μm waveband will be roughly 25 milli-arcseconds. Thus for a canonical system at 10 pc, there will be ≥ 8 fringes spanning the region inside of a 1 AU radius orbit (Fig. 3).

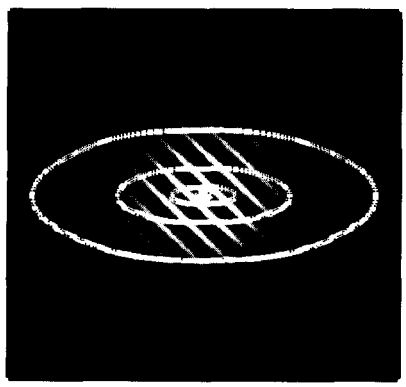

Fig. 3. The Keck Nulling Interferometer's fringe pattern, superposed on white ellipses representing an exozodiacal disk extending out to a radius of 1 AU. Non-normal incidence is considered in this example.

The interferometer's picket-fence transmission pattern (Figs. 3 & 4) will roughly halve the detectable flux from an extended source such as an exozodiacal disk. Furthermore, because the temperature of any exozodiacal disk should rise toward the central stellar position (Fig. 5), the detected exozodiacal emission will be weighted toward the inner parts of the disk.

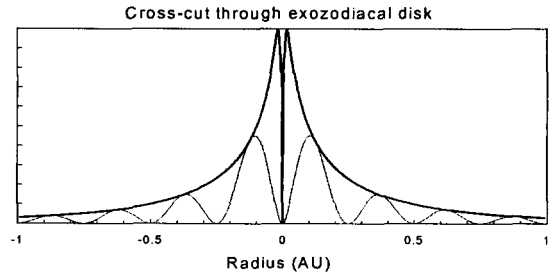

Fig. 4. Cross-cut through an exozodiacal disk as bright as our own zodiacal disk (black), and the product of this model with the KIN's fringe pattern (blue).

Of course planets also increase in temperature with decreasing orbital radius, easing their detection from a signal-to-noise point of view, but making detection more difficult from an angular resolution point of view. Long baselines help in the latter regard, and it turns out that the Keck Interferometer's baseline is long enough to yield a first constructive fringe peak reasonably well-matched to the expected maximum radial offsets of several of the brightest "Hot Jupiters" currently known, especially if somewhat shorter wavelengths near e.g. 5 μm are considered (Fig. 6).

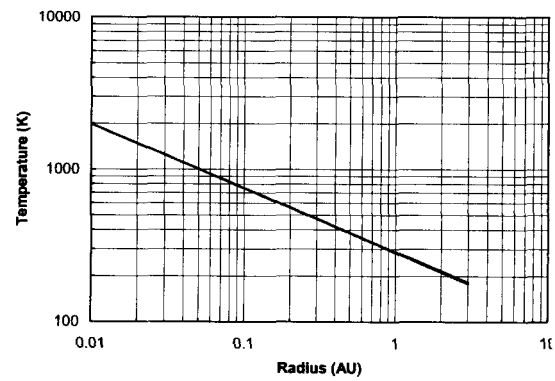

Fig. 5. Zodiacal disk temperature vs. radius.

Fig. 7 compares blackbody emission levels for various temperatures in order to examine the expected contrast ratios. Note that for planets near 1200 K, the contrast ratio near 5 μm is on the order of a part in a thousand. Some theoretical models for planetary atmospheres

actually predict a significant flux enhancement in the relatively transparent 4 to 5 μm wavelength region, making this a particularly promising band for direct detection of close-in Hot Jupiters. Because of the predicted emission enhancement near 5 μm, even non-detections approaching the level of several parts in a thousand would already be able to set stringent constraints on the conditions present in the atmospheres of close-in Hot Jupiters.

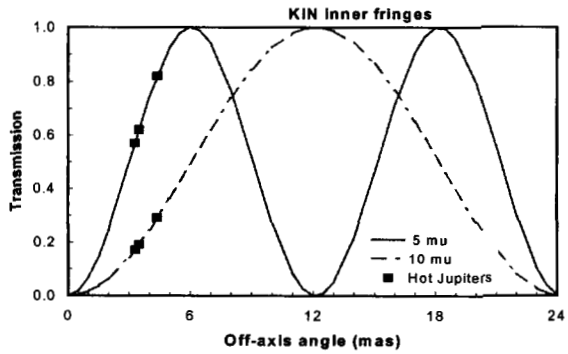

Fig. 6. Maximum elongations of the Hot Jupiters in the τ Boo, 51 Peg, and υ And systems, relative to the Keck fringe patterns at 5 and 10 μm.

Close-in Hot Jupiters also have another significant advantage - short orbital periods. In some cases, the periods are small enough (on the order of four days) to produce an almost daily "on-off" signal modulation as the planet shifts between maximum and minimum elongations (for highly inclined orbits). While operation at wavelengths as short as 5 μm is currently not part of the baseline plan for the KIN's capabilities, a future upgrade to shorter wavelengths could allow this type of observation to be pursued. A final promising area for nulling interferometry is the detection of very young Jupiter-like planets, which have not yet dissipated their heat of formation.

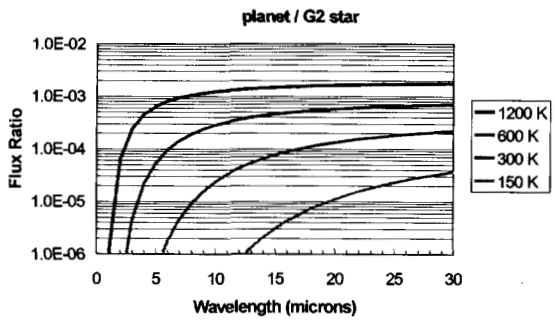

Fig. 7. Blackbody spectral ratios for planets with the listed temperatures, and diameters equal to that of Jupiter.

3. SYSTEM OVERVIEW

Nulling interferometry from ground-based telescopes actually requires a dual suppression of "background" sources, because both the target star and the thermal emission from the terrestrial atmosphere must be removed. For the Keck Interferometer, spatial chopping to remove background emission is not an option at present, so both "backgrounds" will be removed interferometrically.

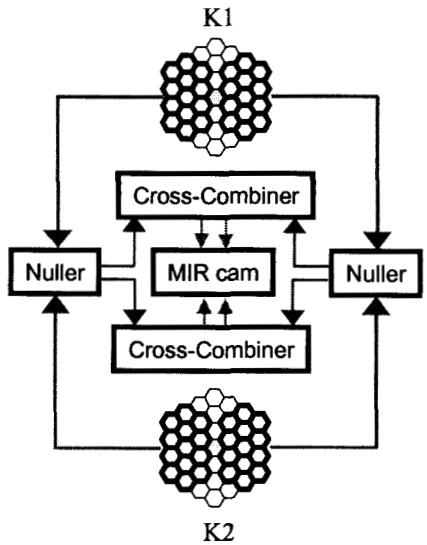

Fig. 8. Architecture of the Keck Interferometer Nuller. Each telescope pupil is divided into two subapertures, shown in bold. Nulling occurs on the pair of long baselines, followed by cross-combination on the short baselines.

To accomplish this dual suppression, each of the Keck telescope pupils will be split into a pair of sub-apertures downstream in the optical train, resulting in four input beams to the interferometer. This approach allows for the sequential removal of both unwanted signals: first stellar nulling is applied on each of the two long parallel baselines between corresponding telescope halves, and then the terrestrial background is removed in a second layer of interferometric "cross-combiners", which combine the light on the short baselines, and which are capable of rapid optical path difference (OPD) modulation (Fig. 8).

The residual light reaching the cross-combiners consists of a coherent part from the extended astronomical source (the leakage from the stellar rim, plus the potential signals from exozodiacal disks and any bright exoplanets present), and a much larger incoherent contribution from the terrestrial atmosphere. By scanning the post-nulling OPD in the pair of cross-

combiners more rapidly than the atmospheric fluctuation timescale, as in a standard interferometric beam-combiner, the residual signal from the astronomical source is converted to an a.c fringe signal, while the incoherent atmospheric background remains at d.c., and so is separated out.

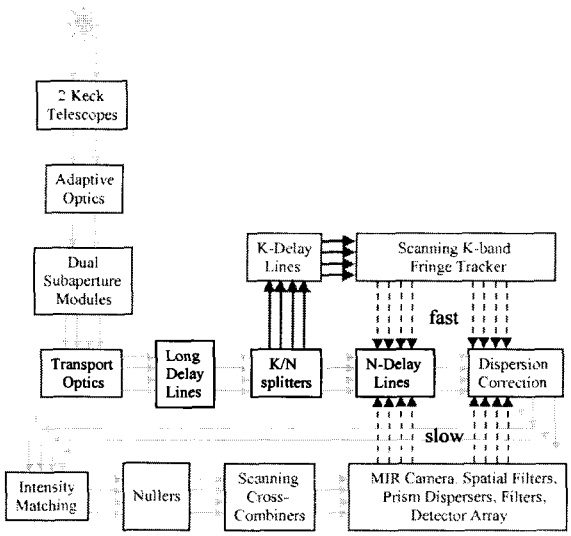

Fig. 9. System level layout of the Keck Interferometer Nuller. The telescopes and associated subsystems (adaptive optics benches and dual-subaperture modules) are shown in maroon, the basement optics prior to the nulling beamcombiner breadboard in black (with the connecting transport optics sharing these two colors), the K-band fringe tracking system in green, the nulling beamcombiner breadboard components in blue, and the N-band camera system in red. The solid arrows are light paths, and the dashed arrows control signals. The update rate from the K-band sensor to the path-length and dispersion correction systems is much higher than from the N-band sensor.

The full optical beam train of the KIN is fairly complex, even in a system-level block diagram (Fig. 9), and can be described as a series of paired subsystems. The first pair of subsystems is of course the Keck telescope pair. This is followed by the Keck adaptive optics (AO) systems on their respective Nasmyth platforms (Fig. 10). After splitting off the visible wavelengths for wavefront sensing on the AO bench with a dichroic beam-splitter, the corrected, collimated infrared beam is sent onward to the dual-subaperture modules (DSMs). These DSMs, located immediately adjacent to the AO benches (Fig. 10), introduce the aperture splits, thus yielding a pair of output beams each, which are then propagated individually from this point onward.

Several transport optics (TO) mirrors next take the four beams under the telescope to the azimuth axis, and on to the beam-combining laboratory in the basement. Each beam then passes through a long delay line (LDL), which serves to take out bulk path differences, and is locked in a stationary position for approximately hour-long timescales. Each beam is next sent onward to a dichroic (K/N) splitter, which separates the near-infrared (J, H, K) and mid-infrared (N) wavebands (more precisely, the mid-infrared band is fully reflected, but the near-infrared light is split roughly equally, to allow for simplified operation with an internal light source).

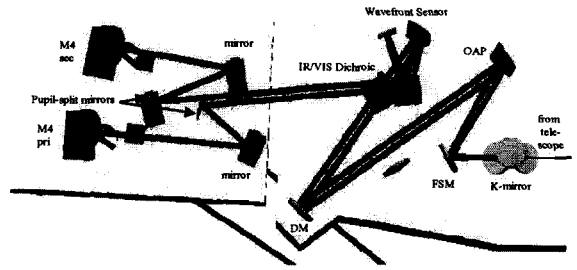

Fig. 10. Keck AO (right) and DSM (left) benches. After the AO bench's off-axis paraboloid (OAP), the infrared beam remains collimated until the FDLs. The aperture split occurs immediately upon reaching the DSM.

Each of the resultant eight beams next goes to a separate fast delay line (FDL), which provides rapid fine-scale path-length compensation. After the FDLs, the beams are compressed in diameter by factor-of-four. The mid-infrared light is then sent on to the nulling beam-combiner (NBC) breadboard (Fig. 11), while the four near-infrared beams are further separated by wavelength, with the K-band light being used for stellar fringe tracking, and the J-band light for angle tracking (pointing).

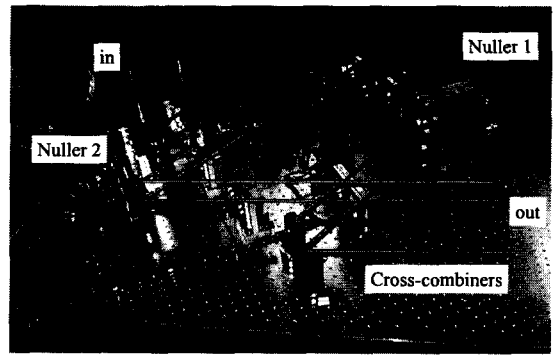

Fig. 11. The KIN's Nulling Beamcombiner (NBC) breadboard. It has four input beams, a pair of nullers, a pair of cross-combiners, and four output beams. The dispersion compensation system, which also mounts on this breadboard, is not shown.

4. PATH-LENGTH COMPENSATION AND STABILIZATION

Because the incident mid-infrared stellar flux is insufficient to stabilize the OPD to the needed degree using only photons in the observing band, OPD stabilization relies on fringe tracking on the stellar signal at near-infrared wavelengths, and on metrology.

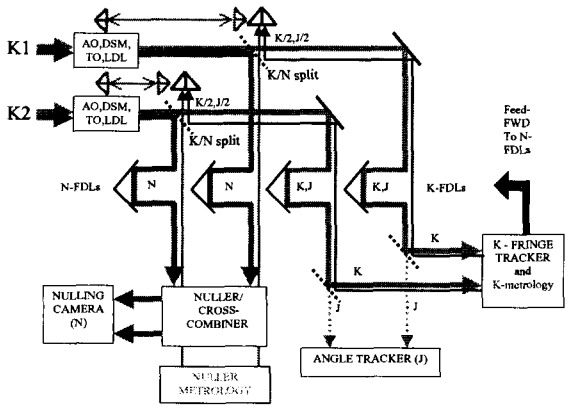

Fig. 12. The Keck Interferometer Nuller stabilization relies on OPD feed-forward from K–band fringe tracker. The red arrows indicate the mid-infrared beams, and the blue arrows the near-infrared beams. The arrows terminating at the triangle-shaped corner cubes are metrology beams.

To stabilize the mid-infrared paths, the near-infrared and mid-infrared wavebands are first separated at the K/N dichroic splitters, after which the two wavebands traverse separate FDLs. The near-infrared FDLs perform repeated OPD scans a wavelength long to accurately locate and track the K-band white-light fringe (WLF) position, and the resultant OPD information is then continually fed to the corresponding mid-infrared FDLs, which passively follow the targeted OPD (Fig. 12).

In the ideal case, the mid-infrared beams would thus arrive at the NBC with an already stabilized phase offset. The correct OPD offset to the mid-infrared WLF position is then determined by temporarily scanning the mid-infrared FDLs in OPD as well, and summing a number of already pre-aligned mid-infrared fringes to build up the signal to noise ratio. After determining the OPD offset to the mid-infrared null fringe, the scanning of the mid-infrared FDLs is stopped, and the N-band null fringe position is held with the continual OPD updates from the still-scanning K-band fringe tracker.

In practice the situation is more complex, because of non-common paths between the mid- and near-infrared beams after the K/N splitters, and time-varying longitudinal atmospheric dispersion. The non-common paths are not a major issue, as they will be stabilized with metrology. Figure 12 outlines the stabilization approach, including metrology, as described to this point, i.e., neglecting variable atmospheric dispersion.

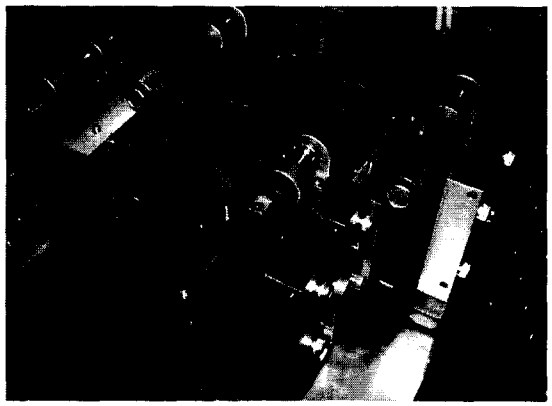

Fig. 13. The KIN's dielectric dispersion compensation system. Each sub-aperture beam traverses a pair of dielectric prisms, which can be translated relative to each other to provide a variable phase dispersion.

However, there are a number of dispersive phase effects that also require compensation. First, the actual beam subtraction inherent in nulling calls for the introduction and steady maintenance of an achromatic phase shift of π radians. Second, the overall path-length difference is compensated not in vacuum, but in air, which results in the introduction of a slowly varying longitudinal dispersion as the source follows its diurnal track. Finally, fluctuations in the amount of water vapor above the two telescopes introduce rapid fluctuations in dispersion.

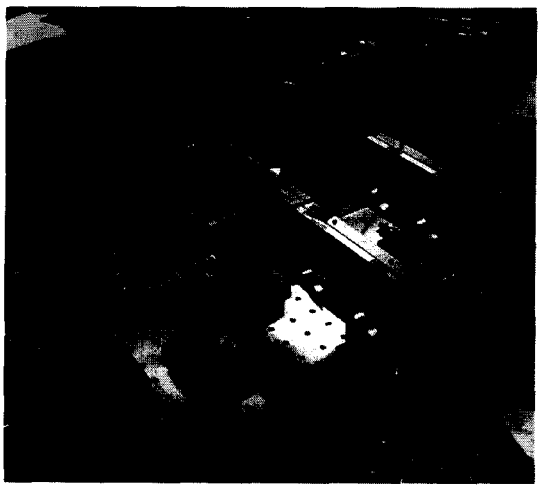

Fig. 14. A JPL modified Mach-Zehnder beam combiner in the laboratory. The beamsplitter substrates are ZnSe, and the mirrors are coated with bare Au.

The atmospheric water vapor fluctuations are expected to be well in excess of π radians, rendering the static π-radian phase shift needed for nulling a relatively minor component of the required phase correction. For this reason, in the ground-based Keck system, the simple field-reversal required for nulling was subsumed into the requisite atmospheric dispersion compensator. As a result, a set of dielectric (ZnSe) prisms (Fig. 13) capable of providing a wide variety of dispersive phase corrections will be used as the dispersion-compensating elements. Note that these elements also correct for mismatches in ZnSe window thicknesses elsewhere in the beam train. Just as is the case for the overall N-band phase, which is controlled largely from the K-band phase, with only slow offset updates from the N-band sensor, so too will the N-band dispersion compensators largely be driven from K-band dispersion measurements, with slower offset updates from the N-band sensor.

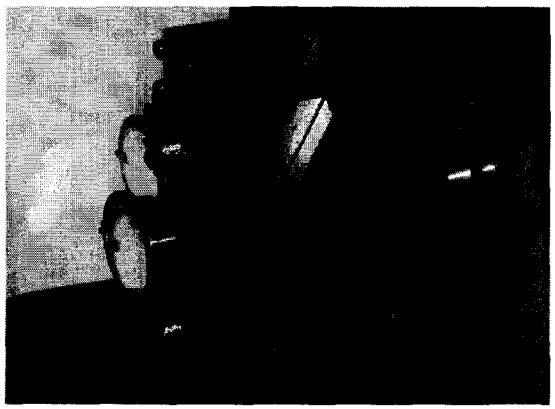

Fig. 15. The "rapid ramp" cross-combiner mirrors.

5. THE NULLING BEAM-COMBINER BREADBOARD

At the heart of the nulling interferometer is the nulling beam-combiner breadboard (Fig. 11). This breadboard, which accepts the four input beams from the four Keck subapertures, consists of a series of optical subsystems of its own: a set of four dispersion correctors (only two of which are actuated), as just described, four intensity control devices (rotatable vanes in the beams), four shutters, a pair of nulling beam combiners, and a pair of cross-combiners. The entire KIN optical system described to this point, through the NBC breadboard, consists of open-air, ambient-temperature optics. The four output beams from the NBC breadboard are then sent onward to a four-beam cryogenic mid-infrared camera for detection of the mid-infrared fringe signals.

The beam-combiners themselves are symmetric, constructive beamcombiners (Fig. 14), based on the modified Mach-Zehnder configuration, in which a pair of reversed beamsplitters allows for the perfect subtraction of incident electric fields which have previously been reversed with respect to each other (in our case by the dispersion compensators).

The cross-combiner design is similar to that of standard astronomical beam-combiners, which consist of a single beam-splitter preceded in one arm by a mirror capable of rapid linear piston ("ramp") motions, with an OPD stroke slightly longer than the wavelength of light under observation. To minimize vibrations, a balanced design is used. The piston mirrors act on collimated light, and so are relatively large (Fig. 15).

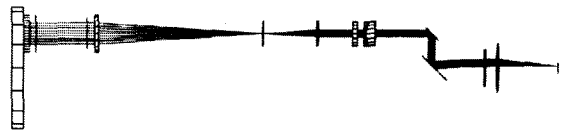

Fig. 16. Optical layout for one of the four KALI beams.

6. THE KALI MID-INFRARED CAMERA

The detection of faint mid-infrared exozodiacal signals also requires an extremely sensitive mid-infrared camera. This camera must also perform several rather specialized functions. The camera must accept four input beams instead of the more usual single beam, and it must be able to be read out more rapidly than the atmospheric fluctuation timescale. To define the beams that are to be interfered, the four-fold beam train of the mid-infrared camera includes a pupil wheel, a focusing lens stage, a pinhole selection stage, a collimating lens

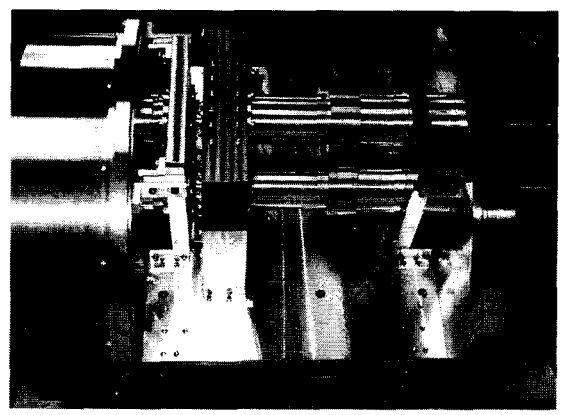

Fig. 17. The KALI camera's four-beam liquid N_2 temperature optical bench assembly.

stage, a filter/polarizer wheel, a (non-deviating) prism wheel, and a quad-periscope system to deliver the four beams onto a single 128 × 128 mid-infrared detector array. Fig. 16 shows the optical layout for one of the four mid-infrared beams. The part of the detector array actually used consists of four small stripes, each fifteen to twenty pixels long, depending on the dispersion selected.

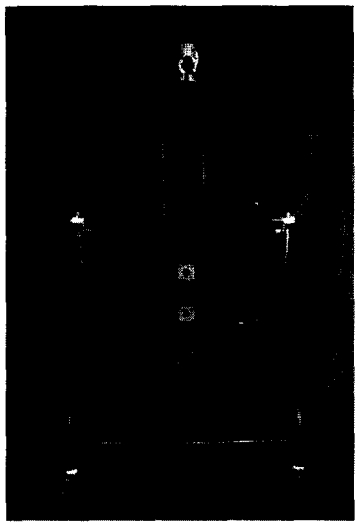

Fig. 18. The four beam mid-infrared camera KALI.

Only the final common lens, the broadband filter, and the mid-infrared detector array (Fig. 16) operate at liquid He temperature, with all of the other optics being on a liquid N_2 temperature optical bench (Fig. 17).

The mid-infrared camera (Fig. 18), dubbed the Keck Aperture nuLling Interferometer camera, or KALI for short, is currently undergoing the final room-temperature end-to-end optical testing, as well as readout electronics testing. Following the successful completion of these phases, the mid-infrared detector array will be inserted, and cold testing will commence.

7. CURRENT PERFORMANCE

The KIN nulling beamcombiner breadboard is now fully assembled (Fig. 11), and the individual subsystems have passed the initial performance verification phase. As can be seen in Fig. 19, one nuller is already performing at the target level specified for the instrument (dual-polarization null depths of about 10^{-4} for thermal white light of ≥ 20% bandwidth). The figure shows periods of steady-state rejection (where rejection is the inverse of null depth) of 5000:1 for a laboratory dual-polarization white-light source (an open-air heated filament) filtered to provide a 29% bandwidth (9.2-12.35 μm). A narrower bandpass (18%) has also been used to obtain somewhat better rejection levels (10,000:1) in the lab. The basic dual-polarization nulling capability of the reversed dual-beamsplitter approach has thus been successfully validated to the 10^{-4} level.

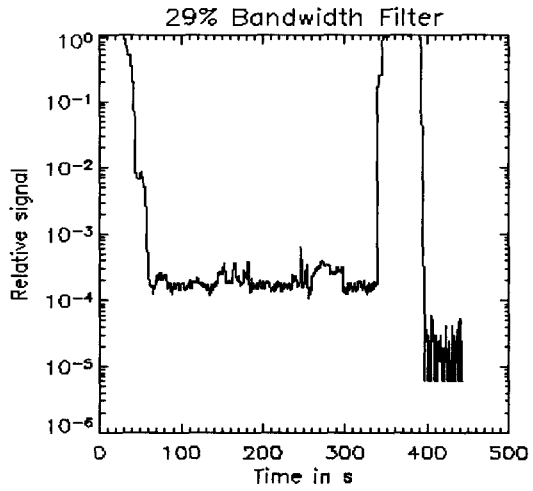

Fig. 19. Nulling of dual-polarization thermal mid-infrared light of 29% bandwidth (9.2 to 12.35 μm). The nulling interferometer was taken from constructive interference to the null fringe (at time ≈ 60 sec) and back (at time ≈ 340 sec), by hand tuning the OPD. At time ≈ 400 sec, the light signal was blocked, allowing detector noise to be measured.

The cross-combiners have also demonstrated the ability to scan with the requisite speed and stroke without disturbing the null stability (recall that the nullers and cross-combiners are on the same optical breadboard), and so are ready for use as well.

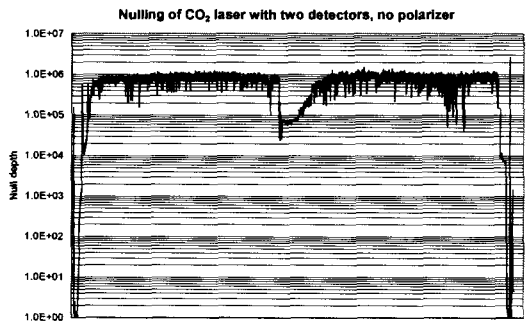

Fig. 20. CO_2 laser nulling at the million to one level.

A second mid-infrared nulling breadboard is also being developed at JPL, under the aegis of the Terrestrial Planet Finder (TPF) project. The goals of this nuller are to demonstrate much deeper (and broader band)

rejection, on the order of a million-to-one. Fig. 20 presents our recent results obtained with this nulling breadboard. As the figure indicates, the TPF nulling breadboard has now reached the targeted million-to-one null-depth level for monochromatic (10.6 μm) CO_2 laser light. Further work to extend to deeper and broader white-light nulls will now be taken over by this breadboard.

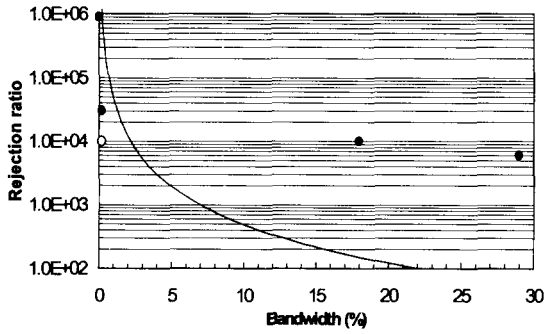

Fig. 21. Best mid-infrared nulling results obtained to date with the JPL nulling beam-combiners.

Fig. 21 provides a summary of the mid-infrared nulling results obtained to date with the symmetric JPL nulling beam-combiners, as a function of bandwidth. For the points at finite bandwidth, the measurements refer to broadband dual-polarization thermal light which has been passed through a bandpass filter. The curve shown in the figure gives the rejection level obtainable by detuning a purely constructive interferometer by half a wavelength (the approach used for our CO_2 laser nulling). Clearly, our broadband nulling results with a reversed beamsplitter pair are well into the achromatic regime.

8. KIN INTEGRATION AND TEST

Because one of the Keck nullers has already met the desired performance specifications, the Keck NBC breadboard is now undergoing integration with the other essential subsystems, including the FDLs, the near-infrared fringe tracker, the metrology subsystem, and the real-time software, in the laboratory at JPL. The final integration phase will involve integration with our mid-infrared camera. All integration steps prior to that will take place using less-sensitive mid-infrared sensors, and will be carried out using only one of the four output beams, so as to progress through the initial integration phases as rapidly as possible. The laboratory integration and test phase is scheduled to be completed later this year, allowing shipment of the nulling instrumentation to the Keck Observatory near the end of the year.

Acknowledgements

I wish to acknowledge the many contributions to this effort of the JPL Keck and TPF nulling teams, including S.L. Crawford, M.J. Creech-Eakman, R. Gappinger, J.M. Geis, G.J. Hardy, C. Koresko, S.R. Martin, B. Mennesson, and J.K. Wallace, as well as of the members of the Keck Interferometer project who have contributed to the definition of the Keck Interferometer Nuller's experimental architecture, including A.J. Booth, P. Dumont, M.M. Colavita, R. Ligon, J. Moore, D.L. Palmer, M. Shao, G.T. van Belle, and G. Vasisht. I also thank M.J. Kuchner for providing Fig. 3. This work was carried out at the Jet Propulsion Laboratory, California Institute of Technology, under contract with the National Aeronautics and Space Administration.